

Comparative Evaluation of Physical and Chemical Beneficiation Routes for Rare Earth Element Recovery from Coal Bottom Ash: A Case Study from Soma Power Plant, Türkiye

Tülin ULUCAN¹, Gülşah GÜVEN¹, N. İlyaz DİNÇ¹, Y. Enes PURAL¹, A. Ekrem YÜCE¹,
Belma SOYDAŞ SÖZER², Fırat BURAT^{1,*}

1. Istanbul Technical University, Faculty of Mines, Mineral Processing Engineering Department, 34469, Maslak, Istanbul, Türkiye

2. Rare Earth Elements Research Institute, Turkish Energy, Nuclear and Mineral Research Agency (TENMAK), Ankara, Türkiye

*Corresponding author: buratf@itu.edu.tr

Abstract

The recovery of rare earth elements (REEs) from coal combustion by-products has attracted increasing attention due to their strategic importance and supply constraints. This study evaluates the recovery potential of REEs from bottom ash (BA) produced by the Soma Thermal Power Plant through an integrated physical–chemical beneficiation route. Characterization indicated that REEs are mainly hosted in aluminosilicate glass and mullite phases, showing limited liberation.

Physical separation methods, including jigging, shaking table, centrifugal (MGS and Knelson), and magnetic separation, achieved only minor enrichment because of the low density and encapsulation of REE-bearing phases. To overcome these limitations, sequential alkaline and acid leaching were employed. Alkaline pretreatment using 5 mol/L NaOH at 90 °C for 4 h partially decomposed the matrix and improved REE accessibility. Subsequent HCl leaching (5 mol/L, 90 °C, 3 h) resulted in the highest \sum REE recovery (>80%) for the –0.106 mm fraction, while 4 mol/L HCl and –0.3 mm conditions provided a more selective and stable extraction.

The combined alkaline–acid leaching process demonstrated a synergistic enhancement in REE mobilization. Overall, sequential chemical leaching offers an effective and scalable approach for REE recovery from coal combustion residues, supporting resource efficiency and waste valorization.

Keywords: Rare earth elements (REEs), Coal bottom ash, Physical beneficiation, Alkaline pretreatment, Sequential chemical leaching, Hydrometallurgical processing, Waste valorization, Soma thermal power plant (Türkiye)

1. Introduction

Rare earth elements (REEs) comprise a group of 15 lanthanides (atomic numbers 57–71), often accompanied by scandium (Sc) and yttrium (Y) due to their similar geochemical and chemical characteristics (Lin et al., 2017). These elements are generally categorized as light (LREE: La–Sm) and heavy (HREE: Eu–Lu), with some classifications including a medium subgroup (MREE: Eu–Y). REEs are indispensable components in numerous strategic applications, including permanent magnets, phosphors, catalysts, and batteries that underpin clean energy, electronics, and defense technologies. Because of their pivotal role in advanced technologies and the concentration of global production, over 85% of which is currently controlled by China, REEs are considered critical raw materials by both the European Commission and the U.S. Department of Energy (Wang et al., 2019; Lin et al., 2017; MTA, 2017). These supply risks have intensified global interest in alternative and sustainable REE sources, especially those derived from secondary resources such as industrial residues and coal combustion by-products. Coal and coal-derived wastes have recently been recognized as promising secondary sources of REEs. The average Σ REE content in coal globally is approximately 60–70 g/t, while coal ashes exhibit significantly higher concentrations, averaging around 400 g/t (Zhang et al., 2017; Lin et al., 2017). Certain coal basins in Russia, the United States, and Canada have reported REE contents exceeding 1000 g/t. In Türkiye, REE contents in coals average 116 g/t, nearly double the global mean, though still below the economic recovery threshold of 800–900 g/t (Zhang et al., 2015; Lin et al., 2017). Studies by Karayığit et al. (2000) confirmed that REEs in Turkish thermal coals predominantly occur in inorganic mineral phases, implying that coal combustion residues such as fly ash and bottom ash can serve as suitable feedstocks for REE extraction. These residues represent abundant, low-cost secondary resources that, if properly processed, could both reduce waste disposal impacts and support critical material independence.

However, REE extraction from coal ashes faces two principal challenges: (i) limited mineral liberation due to encapsulation within amorphous aluminosilicate glass phases, and (ii) weak selectivity of physical beneficiation methods. Physical separations such as gravity, magnetic, and flotation processes serve mainly as pre-concentration steps but remain constrained by the ultrafine (<5 μ m) nature of REE-bearing phases (Dai et al., 2012; Pan et al., 2020). For instance, while physical concentration can improve REE grades moderately, from ~782 ppm to ~1025 ppm in fly ash, acid leaching steps are typically required to achieve extraction efficiencies above 80% (Pan et al., 2020). Bottom ash, due to its coarser texture and lower surface reactivity, generally exhibits even less enrichment potential (Gao & Chen, 2010; Dai et al., 2012).

Magnetic separation, particularly wet high-intensity magnetic separation (WHIMS), can isolate paramagnetic REE-bearing minerals such as monazite and xenotime (Honaker et al., 2016). Nonetheless, recovery rates typically remain below 2% owing to small particle sizes and low mass yields, indicating that physical separation alone is insufficient for substantial REE enrichment.

To overcome the limited liberation and weak selectivity of purely physical routes, physical separations are frequently integrated with thermal activation and alkali–acid hydrometallurgical treatments to enhance REE accessibility. Thermal activation between 400 and 800 °C enhances mineral reactivity by dehydroxylating kaolinite to metakaolinite, breaking amorphous aluminosilicate networks, and increasing surface area and porosity (Stoy et al., 2021). In bottom ash where REEs are mostly hosted in Al–Si glass or mullite phases, such structural rearrangements are critical for subsequent leaching. Alkaline pretreatment using NaOH or Na₂CO₃ targets the refractory aluminosilicate matrix by converting insoluble silicates into soluble or metastable sodium silicates and aluminates, thus exposing REE-bearing microdomains and improving acid reactivity (Trinh et al., 2022). Morphological analyses after NaOH treatment reveal enlarged pores, etched surfaces, and enhanced corrosion features, while XRD patterns show a decline in Al and Si peak intensities evidence of partial matrix dissolution. Under conditions of 5 M NaOH, 90 °C, 120–240 min, and L/S ≈ 10:1, up to ~50 % of the ash matrix dissolves or converts to soluble forms, substantially improving REE accessibility.

Following alkali activation, acid leaching with HCl facilitates REE mobilization via proton attack and chloride complexation. Trinh et al. (2022) reported that pretreatment with 5 M NaOH at 100 °C doubled the REE concentration and enabled > 90 % recovery with 5 M HCl at 50 °C. Similar sequences have yielded recoveries above 75% (Zhang et al., 2020). For silica-rich ashes, alkali roasting followed by organic acid leaching (e.g., citric acid) provides recoveries between 70–84%, depending on mineralogy.

Optimization studies highlight 5 M HCl, 50–90 °C, 120–180 min as the most effective window for maximizing REE dissolution (King et al., 2018; Trinh et al., 2022). A practical limitation of the alkaline step is silica gel formation, which can hinder REE dissolution by blocking diffusion pathways; however, this can be mitigated by controlling NaOH concentration, maintaining moderate L/S ratios, or introducing Na₂CO₃ or mild carbonation (King et al., 2018). Efficient hot filtration or decantation before acid leaching also minimizes gel carryover.

Overall, the sequential thermal–alkali–acid process effectively disrupts the aluminosilicate framework, exposes encapsulated REEs, and increases their solubility, commonly achieving

80–90 % recovery under optimized conditions (Stoy et al., 2021; Wen et al., 2020; Trinh et al., 2022; Zhang et al., 2020). Despite extensive research on REE extraction from fly ash, bottom ash remains largely underexplored, particularly in the context of Turkish lignite-fired power plants. This study represents the first comprehensive investigation of REE recovery from Soma bottom ash in Türkiye, combining physical beneficiation with sequential alkaline and acid leaching. The integrated approach not only elucidates the geochemical behavior and processability of REEs within bottom ash matrices but also establishes a scalable and sustainable process framework that can be adapted for similar residues worldwide. By demonstrating that Turkish lignite-derived bottom ash can serve as a viable secondary resource for critical materials, this work contributes a novel and regionally significant perspective to the global REE recovery research field.

2. Materials and methods

2.1. Material

The Soma Lignite Basin, located in western Türkiye, comprises a thick Miocene–Pliocene sedimentary succession that unconformably overlies a Mesozoic carbonate basement. The Soma Formation comprises alternating clastic and lignitic members, while the overlying Deniz Formation includes volcanoclastic and carbonate units with a wider areal extent and greater lithological variability. The contact between them is marked by a sedimentary unconformity, reflecting a break in deposition and a shift from clastic to volcanoclastic sedimentation (Alan et al., 2014). Overall, this stratigraphic framework reflects alternating phases of subsidence and sediment supply that governed lignite accumulation and mineralogical heterogeneity within the basin. The lignite is typically hard, black, and lustrous, with thin interbeds of coal and lignitic laminae, indicative of deposition in a low-energy lacustrine to swamp environment with episodic clastic influx (Whateley, 1995).

The Soma basin hosts two major thermal power plants. The Soma Thermal Power Plant consumes approximately 8 million tons of coal annually, producing nearly 3.6 million tons of ash as a byproduct. The plant consists of six units, each rated at 165 MW, with a total installed capacity of 990 MW. Units 1–4 burn coal with a calorific value of 2400 kcal/kg, while Units 5–6 utilize lower-grade coal (1550 kcal/kg) supplied by the Turkish Coal Enterprises (TKİ) – ELİ Soma mines (Url-1). The bottom ash (BA) sample used in this study was supplied from the Soma Thermal Power Plant operated by Konya Şeker Sanayi ve Ticaret A.Ş., located in the Soma district of Manisa, Türkiye. Approximately 500 kg of bottom ash was collected and homogenized at the Prof. Dr. Güven Önal Pilot Plant of Istanbul Technical University's Mineral

Processing Engineering Department. Representative sub-samples were obtained using a riffle splitter. Prior to experimentation, all samples were oven-dried at 105 °C for 24 h and stored in sealed containers to prevent moisture adsorption and carbonation. Particle size distribution was determined by dry sieve analysis, and three different fractions were prepared for testing: the as-received sample (~1 mm), <0.3 mm, and <0.150 mm. These fractions were employed to examine the influence of particle size on the physical beneficiation and chemical extraction behavior of REEs.

As part of the characterization studies, the ash content of the sieve-fractioned samples was determined following the ASTM D6357 standard procedure. The total ash content of the as-received bottom ash sample was found to be 92.15 wt%, reflecting the highly inorganic and refractory nature of the material. The Σ REE concentration of the same sample was measured as 141 g/t, which is consistent with the range reported for coal-derived ashes of similar composition. For the chemical enrichment tests, alkaline and acid leaching experiments were conducted under controlled laboratory conditions. Sodium hydroxide (NaOH, $\geq 99\%$, Tekkim, Türkiye) and hydrochloric acid (HCl, 37%, ISOLAB, Germany) were used as leaching reagents.

2.2. Characterization

Mineralogical, chemical, and morphological characteristics of the BA samples were comprehensively analyzed. To determine the particle size distribution, a wet sieve analysis was performed on the BA sample. Based on the cumulative undersize curve, the d_{80} and d_{50} values were determined to be 0.98 mm and 0.42 mm, respectively. X-ray diffraction (XRD) analysis was performed using $\text{CuK}\alpha$ radiation ($2\theta = 5\text{--}80^\circ$), and X-ray fluorescence (XRF) was used to determine the bulk oxide composition. Rare earth element contents were quantified using inductively coupled plasma mass spectrometry (ICP-MS, Agilent 7800) after lithium borate fusion digestion to ensure complete dissolution of REE-bearing phases.

For REE analysis via ICP-MS, the lithium borate fusion method was utilized to ensure complete dissolution of REE-bearing minerals. Prior to chemical analysis, both the particle size fractions obtained from sieve analysis and the physically enriched bottom ash products were prepared in accordance with the ASTM D6357 standard. According to this procedure, the dried samples were first ground in a ring mill to a particle size below 150 μm and subsequently ashed. Approximately 0.5 g of ash was obtained by weighing an appropriate amount of material with a precision of ± 0.1 mg using a 50 mL clear quartz or high-silica crucible. The crucible was placed in a cold muffle furnace programmed to reach 300 °C within the first hour and 500 °C within the second hour. The ashing process continued at 300 °C for one hour, followed by two

hours at 500 °C. After this initial step, the sample was stirred and subjected to an additional hour of ashing at 500 °C to ensure complete combustion. Upon completion, the samples were cooled either in a desiccator or inside the closed muffle furnace to avoid rehydration, and the final ash mass was determined gravimetrically (Url-2).

Given that the bottom ash samples had already undergone high-temperature combustion (> 800 °C) during power-plant operation, this additional ashing step was not intended for complete oxidation but rather to remove minor residual organics and achieve matrix homogeneity. Therefore, a controlled low-temperature ashing (LTA) approach at 500 °C was adopted, consistent with the upper thermal limit recommended by ASTM D6357 for trace-element determination in coal-derived residues. The selection of 500 °C was made to minimize the volatilization of light rare earth elements (REEs) and other volatile trace metals, which are known to be lost at higher temperatures. Several studies have reported that excessive ashing temperatures ($\geq 800\text{--}850$ °C) can promote the decomposition of REE-bearing chlorides, sulfates, and carbonates, resulting in analytical underestimation during subsequent ICP–MS measurement (Dai et al., 2012; Wang et al., 2019). Furthermore, high-temperature ashing may induce recrystallization of amorphous aluminosilicate matrices, causing encapsulation or reorganization that impedes complete leaching and digestion (Thomas et al., 2024).

XRD analysis (Figure 1) revealed that the BA sample exhibited a predominantly crystalline structure characterized by strong reflections of calcite (CaCO_3) and quartz (SiO_2), with subordinate amounts of gypsum ($\text{CaSO}_4 \cdot 2\text{H}_2\text{O}$), illite $[(\text{K},\text{H}_3\text{O})(\text{Al},\text{Mg},\text{Fe})_2(\text{Si},\text{Al})_4\text{O}_{10}(\text{OH})_2 \cdot (\text{H}_2\text{O})]$, and anorthite ($\text{CaAl}_2\text{Si}_2\text{O}_8$). The intense calcite peak at $2\theta \approx 29^\circ$ and quartz peak at 26.6° indicate the predominance of Ca–Si phases, consistent with coal combustion under suboxidizing conditions. The relatively low amorphous background suggests limited glassy phase formation, which could positively influence REE leachability by reducing encapsulation within amorphous silicate matrices and improving acid accessibility.

The XRF analysis (Table 1) confirmed a composition enriched in CaO (38.6%) and SiO_2 (29.9%), followed by Al_2O_3 (9.4%) and Fe_2O_3 (8.2%), reflecting a calcium–aluminosilicate-type ash with a significant iron oxide fraction. The Fe_2O_3 content supports the XRD indication of ferruginous minerals, consistent with the potential magnetic susceptibility observed during beneficiation, confirming the presence of paramagnetic phases that respond to high-intensity magnetic separation. Minor oxides such as MgO (2.1%), K_2O (0.8%), and Na_2O (0.5%) suggest the presence of clay-derived minerals.

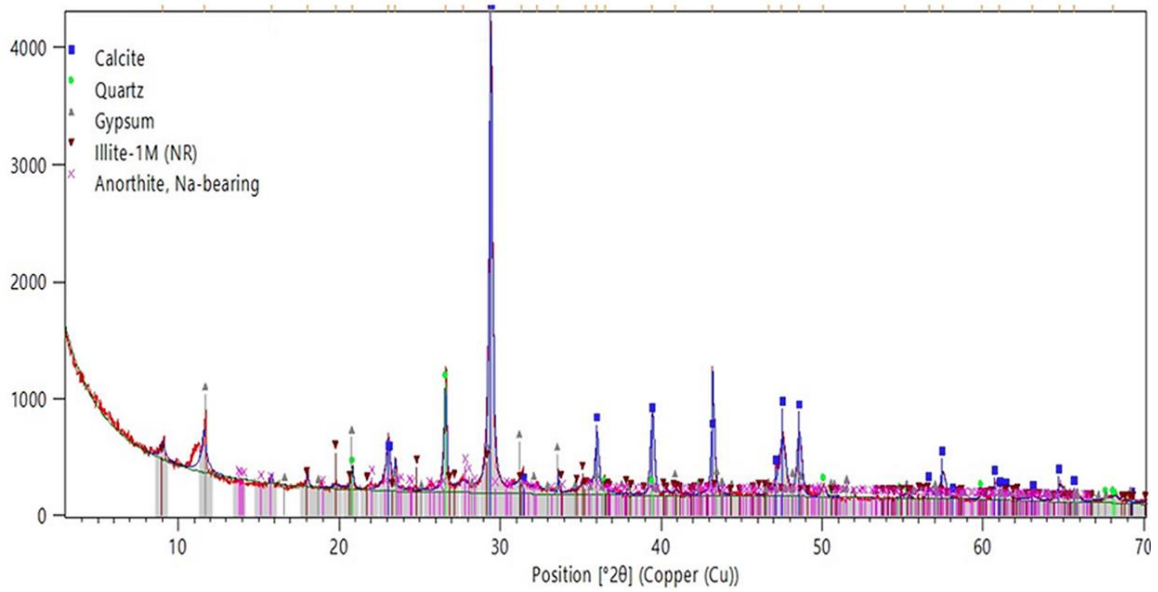


Figure 1. XRD analysis of BA.

Table 1. The main oxide compositions and contents of the BA.

Major elements (wt.%)			
CaO	38,6	MgO	2,1
SiO ₂	29,9	K ₂ O	0,8
Al ₂ O ₃	9,4	TiO ₂	0,3
Fe ₂ O ₃	8,2	Na ₂ O	0,5

Based on the REE analysis results of the non-ashed feed sample, (Table 2), the Σ REE concentration in the Soma BA was 122.7 g/t, with REEs such as Ce (37.2 g/t), La (25.0 g/t), and Nd (18.9 g/t) being the most abundant. HREEs like Y (16.3 g/t), Dy (2.8 g/t), and Gd (3.3 g/t) were present in lower amounts, yielding an LREE/HREE ratio of approximately 3.8. This distribution pattern is typical of coal-derived ashes dominated by aluminosilicate and calcium phases (Dai et al., 2012). The observed REE concentrations exceed the global average for coal ashes (\approx 400 g/t), indicating that the Soma bottom ash represents a potentially valuable secondary REE resource in Türkiye. According to the chemical analysis results of the particle size fractions, the bottom ash sample contains a total of 141 g/t REEs on an ash basis. The combined major oxide and Σ REE contents across the particle size fractions of the bottom ash sample are presented in Figure 2.

Table 2. REE contents of the BA.

Elements	Sc**	La**	Ce**	Pr**	Nd**	Sm**	Ey*	Gd*	
Content (g/t)	0.23	24.97	37.23	4.68	18.98	3.74	1.06	3.26	
Elements	Tb*	Dy*	Ho*	Er*	Tm*	Yb*	Lu*	Y*	Σ REE***
Content (g/t)	0.51	2.80	0.57	1.68	0.27	0.27	1.62	16.26	122.7

*HREE: Heavy Rare Earth Elements; **LREE: Light Rare Earth Elements; *** Σ REE: Total REE

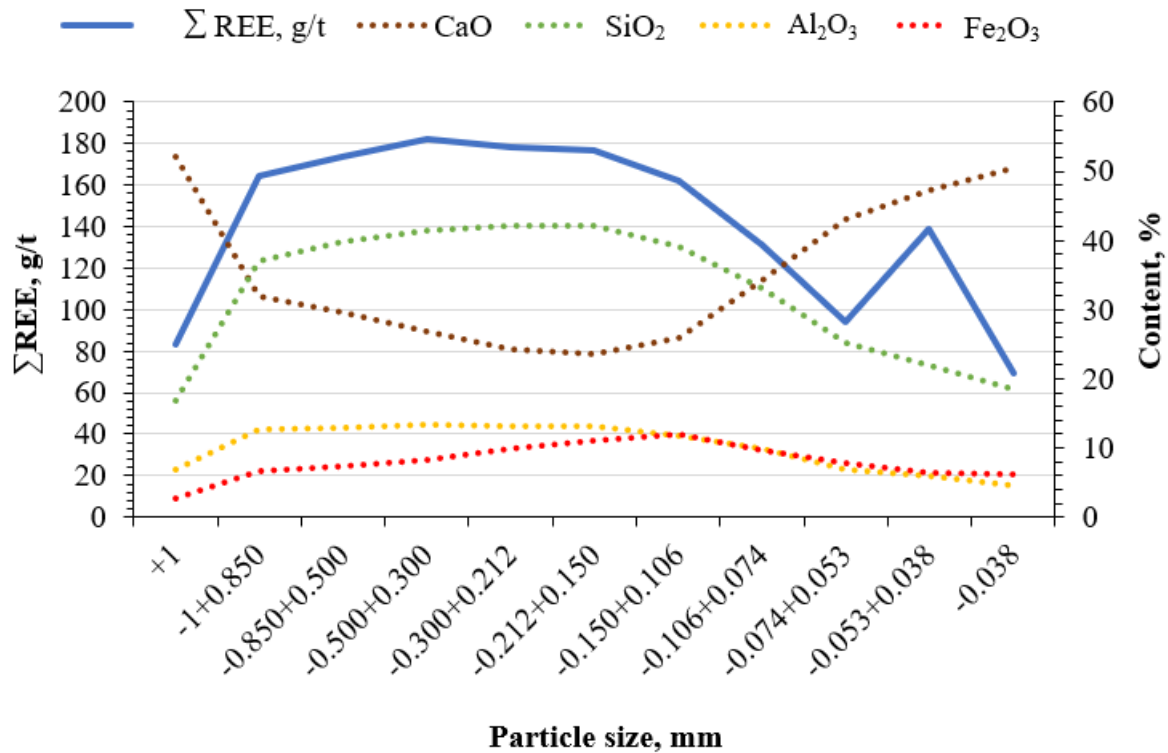


Figure 2. Combined major oxide and Σ REE contents across particle size fractions of the BA.

The variation of major oxide compositions and Σ REE contents across particle size fractions of the BA provides valuable insight into the mineralogical heterogeneity and REE-hosting behavior of the material. As shown in Figure 2, Σ REE concentrations exhibit a distinct size-dependent trend, reaching maximum values in the intermediate size fractions ($-0.5+0.212$ mm and $-0.212+0.150$ mm), followed by a marked decline in the coarser and finer ranges. This distribution suggests that REE-bearing phases are predominantly associated with medium-density particles that correspond to partially liberated aluminosilicate glass and mullite phases, rather than coarse, refractory mineral grains or ultra-fine amorphous materials.

Among the major oxides, CaO and SiO₂ show inverse trends CaO increases toward coarser sizes, whereas SiO₂ becomes dominant in finer fractions. This indicates that calcium-rich

phases, possibly derived from calcite or anorthite decomposition products, tend to concentrate in larger particles, while finer fractions are enriched in silicate glassy materials. Al_2O_3 content progressively increases from coarse to fine sizes, reflecting the concentration of aluminosilicate and clay-derived phases at smaller particle sizes. The Fe_2O_3 content remains relatively low but exhibits minor fluctuations, implying the dispersed presence of iron-bearing oxides or spinel-type minerals across all size ranges.

The observed decrease in $\sum\text{REE}$ content in the finest fractions (-0.053 mm and below) may be attributed to the dominant presence of amorphous, low-density Si–Al glass, in which REEs are more uniformly distributed but less concentrated. Additionally, finer particles often include unburned carbon or secondary reaction products formed during combustion, which dilute the apparent REE concentration. Conversely, the enrichment peak in the mid-size range implies partial liberation and aggregation of REE-bearing aluminosilicate fragments, which are known to host REEs through isomorphic substitution or surface adsorption.

Overall, the data confirm that REE distribution in bottom ash is controlled by both mineralogical associations and particle size dependent liberation characteristics. The predominance of REEs within medium-size fractions supports the selection of this range for targeted beneficiation, as it combines favorable density, magnetic response, and leaching reactivity.

2.2. Methods

In this study, a combined approach integrating physical and chemical separation methods was applied to assess the potential for recovering REEs from BA generated by the Soma Thermal Power Plant in Türkiye. Physical beneficiation focused on concentrating REE-bearing minerals by exploiting density and magnetic contrasts, while chemical extraction targeted the dissolution of REEs through alkaline and acid leaching techniques.

2.2.1. Physical Separation

Physical enrichment was performed using density-based and magnetic separation techniques. The density-based separations included a jig, Wilfley-type shaking table, and centrifugal concentrators specifically a Multi Gravity Separator (MGS) and a Knelson concentrator selected for their effectiveness in processing coarse-to-fine coal combustion residues, as previously reported by Pan et al. (2020) and related studies. Based on particle size, the sample was classified into three main fractions using 1 mm and 0.3 mm sieves:

- Particles > 1 mm were processed by jigging,

- $-1 + 0.3$ mm fraction was treated on the Wilfley-type shaking table, and
- <0.3 mm fraction was processed with the MGS and Knelson centrifugal concentrators.

In the shaking table experiments, the pulp solids ratio (PSR) was maintained at 20%, with a wash water flow rate of 3 L/min, a table inclination of 0° , and a stroke amplitude of 15 mm. For the MGS tests, the samples were conditioned at a 10% PSR, while the drum rotational speeds were adjusted to 280, 260, and 250 rpm, respectively. The wash water flow rates were set to 1, 3, and 5 L/min, and the drum vibration amplitude and inclination were maintained at 15 mm and 0° , respectively. For the Knelson concentrator experiments, the feed samples were also prepared at a 10% PSR and introduced into the concentrator in a batch mode, while the fluidization water pressure was controlled within the ranges of 0.5–3 psi during the tests.

Additional tests were conducted on finer size classes (-0.106 mm and -0.038 mm) to evaluate the performance of centrifugal devices for ultrafine fractions. Magnetic separation was applied to three particle-size intervals ($-1+0.5$ mm, $-0.5+0.212$ mm, and -0.212 mm). The coarser fractions ($-1+0.5$ mm and $-0.5+0.212$ mm) were processed using a REMS high-intensity dry belt magnetic separator operating at a belt speed of 120 rpm, with splitter blade angles between 95° and 125° . The fine fraction (-0.212 mm) was treated using a Carpcow wet high-intensity magnetic separator, where the magnetic field intensity was varied between 4 and 6 amperes.

This multistage approach enabled the selective concentration of paramagnetic REE-bearing phases (e.g., monazite, xenotime, allanite) and the removal of non-magnetic silicate gangue, providing optimized feed material for subsequent chemical extraction.

2.2.2. Chemical Separation

Following physical enrichment, chemical leaching experiments were conducted to evaluate REE extraction efficiency. The objective was to liberate REEs from refractory aluminosilicate matrices and enhance their solubility through sequential alkaline pretreatment and acid leaching. Alkaline leaching was performed using sodium hydroxide (NaOH) to partially dissolve the glassy aluminosilicate phase typical of coal combustion residues. The optimal operating parameters were determined as: NaOH concentration = 5 mol/L, temperature = 90°C , leaching duration = 4 h, liquid-to-solid ratio = 8:1, and stirring speed = 800 rpm (Table 3). These conditions are consistent with prior studies that demonstrated the ability of NaOH to disrupt aluminosilicate networks and increase the accessibility of encapsulated REEs (Wen et al., 2020; King et al., 2018). Subsequently, acid leaching was conducted on the pretreated samples using hydrochloric acid (HCl) at concentrations of 3, 4, and 5 mol/L, maintaining 90

°C temperature, 3 h leaching time, 10:1 liquid-to-solid ratio, and 400 rpm stirring speed (Table 3).

Table 3. Alkaline leaching and acid leaching test conditions.

		Leaching test conditions		
Alkaline Leaching (NaOH)	Concentration, mol/L	5 mol/L		
	Temperature, °C	90°C		
	Time, h	4 h		
	Liquid: Solid ratio	8:1		
Acid Leaching (HCl)	Concentration, mol/L	3 mol/L	4 mol/L	5 mol/L
	Temperature, °C	90°C	90°C	90°C
	Time, h	3 h	3 h	3 h
	Liquid: Solid ratio	10:1	10:1	10:1

3. Results and Discussion

The experimental results are presented and discussed in this section to evaluate the REE recovery potential from Soma bottom ash through an integrated beneficiation leaching approach. The findings are organized into two main stages: physical enrichment, based on density and magnetic separation, and chemical extraction, involving sequential alkaline and acid leaching.

3.1. Enrichment of REEs by Physical Methods

Physical beneficiation techniques such as gravity, magnetic, and electrostatic separations are commonly applied to increase the concentration of REEs in coal combustion residues. These methods utilize differences in specific gravity and magnetic susceptibility to selectively separate REE-bearing minerals from silicate gangue. In the case of Soma bottom ash, gravity-based processes (jigging, shaking table, and centrifugal separation) were employed to concentrate denser mineral fractions, while magnetic separation was used to recover paramagnetic REE-bearing phases associated with ferruginous minerals. The combined approach provided a preliminary concentration of REEs prior to chemical extraction.

3.1.2. Gravity separation

Gravity separation, particularly jigging, has proven effective for the enrichment of REEs from coal bottom ash by exploiting differences in particle density. This method enables the separation of coarse mineral fractions, concentrating heavier REE-bearing particles while rejecting lighter silicate gangue. Previous studies have shown that jigging can enhance REE concentrations up

to twofold, with recoveries generally exceeding 65%, depending on particle size distribution and operating conditions (Pan et al., 2020; Zhang et al., 2020).

In the present study, jigging was applied to the +1 mm fraction of the Soma bottom ash sample to evaluate its potential for preliminary REE upgrading. The results of the jig beneficiation experiments are summarized in Table 4, which demonstrate the efficiency of density-based separation in concentrating REE-bearing mineral phases prior to fine gravity and magnetic processing.

Table 4. Jig test result at + 1 mm size.

Products	Amount, %	Ash, %	ΣLREE, g/t	ΣHREE, g/t	ΣREE, g/t	ΣREE Distribution, %
Heavy 1	22.6	95.7	17	39	56	14.8
Heavy 2	21.0	93.8	20	51	71	17.4
Middling	38.1	92.3	23	61	84	37.4
Light 1	8.1	75.7	34	94	128	12.1
Light 2	10.2	81.9	40	114	154	18.3
Total	100.0	91.0	24	62	86	100.0

The jig beneficiation experiment produced five distinct product fractions: Heavy 1, Heavy 2, Middling, Light 1, and Light 2. As summarized in Table 4, the light fractions collectively exhibited the highest Σ REE concentration, reaching 154 g/t in the Light 2 product with a recovery of 18.3%.

Interestingly, REEs were preferentially enriched in the light fractions, contrary to expectations based solely on density contrast. This trend is attributed to mineralogical transformations occurring during coal combustion. Previous studies have reported that clay minerals such as kaolinite and illite decompose and transform into mullite and amorphous Si–Al glass phases, leading to the redistribution of REEs within these newly formed matrices (Dai et al., 2012; Pan et al., 2020). These glassy and mullite-rich phases possess lower effective densities compared to conventional heavy minerals, causing REE-bearing particles to preferentially accumulate in lighter products during jigging.

Moreover, the occurrence of unburned carbon, often agglomerated with clay minerals, may further decrease apparent particle density and facilitate REE association with light fractions. Consequently, the jigging results indicate that REE partitioning is influenced not only by specific gravity contrasts, but also by the combustion-induced mineralogical evolution of the

ash matrix and the residual carbon content, which collectively control the density-based behavior of REE-bearing particles.

In the shaking table tests, Σ REE concentration in the heavy fraction reached 130 g/t, corresponding to a 47.0 % recovery, while the light fraction contained 136 g/t. This minimal difference indicates that the shaking table achieved no significant REE enrichment for this size range. The MGS tests showed only limited REE upgrading in the heavy products. For the -0.3 mm feed, the heavy fraction contained 187 g/t REEs, while the light fraction had 137 g/t; however, 40.9% of REEs were distributed in the middling fraction. At -0.106 mm, the heavy product yielded grades of 145–168 g/t with an overall recovery of 69.1%, still indicating modest enrichment. These results indicate that while MGS can partially concentrate REEs into the heavy products at finer size fractions, mineralogical associations and incomplete liberation limit the expected grade improvement.

It was determined that separation based solely on specific gravity differences using the MGS centrifugal separator is insufficient for effective REE recovery. Therefore, enrichment experiments employing other centrifugal separators capable of generating significantly higher G-forces than the MGS were initiated. In the Knelson centrifugal separator experiments conducted on -0.3 mm, -0.106 mm, and -0.038 mm size fractions, it was revealed that there were size-dependent variations in the distribution of REEs among the products. At the -0.3 mm feed size, the heavy fraction achieved a modest enrichment, containing approximately 187 g/t REEs and accounting for 41.0% of the total recovery. In the -0.106 mm fraction, the heavy product reached the highest grade of 204 g/t; however, this fraction represented only 10.1% of the total recovery, with the majority of REEs reporting to the light (60.9%) and middling (28.9%) products. For the -0.038 mm fraction, the highest grade was observed not in the heavy product but in the middling fraction (197 g/t), while the heavy fraction contained only 158 g/t with a recovery of 6.3%. These results indicate that although the Knelson concentrator can partially enrich REEs into the heavy fraction at coarser sizes, at finer sizes mineralogical associations, the low effective density of glassy phases, and the hydrodynamic behavior of fine particles cause REEs to be preferentially partitioned into the middling and light fractions rather than the expected heavy product.

When the results of the MGS and Knelson experiments are considered together, both techniques produced only limited grade improvements in REEs, while exhibiting distinct trends in their distribution. These findings indicate that REEs in bottom ash do not behave like conventional heavy minerals, owing to their predominant occurrence within amorphous Al-Si glass phases

and mullite formed during combustion. Similar observations have been reported in the literature, where REEs in coal-derived ashes could typically be enriched by only 1.1–1.5 times through density-based methods and were largely concentrated in fine, non-magnetic, and medium-density fractions (Pan et al., 2020; Abaka-Wood et al., 2022).

3.1.2. Magnetic separation

Magnetic separation tests were performed on three size fractions ($-1+0.5$ mm, $-0.5+0.212$ mm, and -0.212 mm) using both REMS and Carpco high-intensity separators, and the results are summarized in Table 5. For the $-1+0.5$ mm fraction treated by the REMS dry separator, the magnetic product constituted only 1.9 % of the total mass with an ash content of 95.9 %, yielding a \sum REE concentration of 182 g/t. The non-magnetic product, representing 4.3 %, contained 58 g/t \sum REE, indicating only a modest enrichment in the magnetic fraction.

Table 5. Soma Thermal Power Plant bottom ash sample magnetic separation test results.

Particle size, mm	Amount, %	Products	Content REE, g/t	Distribution, %	Ash, %	According to the experiment	
						REE content, g/t	REE Distribution, %
$-1+0.5$ (REMS)	28.7	Magnetic	190	1.9	95.9	182	2.4
		Middling	179	16.3	95.4	171	20.9
		Non-Magnetic	61	4.3	94.3	58	5.5
		Total	131	22.5	95.0	124	28.8
$-0.5+0.212$ (REMS)	37.0	Magnetic	206	5.0	93.7	193	5.1
		Middling	203	24.0	91.7	186	24.2
		Non-Magnetic	97	7.7	91.0	88	7.7
		Total	166	36.7	91.6	152	37.0
-0.212 (Carpc)	34.3	Magnetic	313	9.4	95.2	298	8.2
		Middling	351	3.4	92.9	326	2.6
		Non-Magnetic	169	28.0	91.1	154	23.4
		Total	199	40.8	91.8	182	34.2
Total	100.0		167	100.0		154	100

A similar trend was observed in the $-0.5 + 0.212$ mm size range, where the magnetic product showed 193 g/t \sum REE compared with 88 g/t in the non-magnetic portion. Although the REE grade was slightly higher in the magnetic product, overall recoveries remained low, suggesting that only a portion of REE-bearing minerals exhibit magnetic response at this size.

More distinct behavior was observed for the -0.212 mm fraction separated by the Carpcow wet high-intensity magnetic separator (4–6 A). The magnetic fraction, accounting for 9.4 % of the mass, achieved a significantly enhanced Σ REE content of 313 g/t, while the non-magnetic fraction (28.0 %) contained 169 g/t. These results demonstrate that finer particle sizes enhance REE association with weakly magnetic phases, likely due to mineralogical transformations during combustion.

The observed magnetic response of REE-bearing phases can be attributed to several mechanisms:

- (i) Thermal transformations during coal combustion cause the conversion of REE-hosting silicates and phosphates into oxides or Fe-bearing glassy phases with weak paramagnetic properties;
- (ii) Alterations in magnetic behavior may arise from Fe substitution or defect formation within aluminosilicate matrices, enhancing their response to high-intensity fields; and
- (iii) Encapsulation of REEs within Fe-bearing particles during melting and solidification can result in indirect magnetic recovery.

Overall, magnetic separation achieved partial REE enrichment, particularly at finer size fractions, confirming that REEs are mainly associated with paramagnetic or weakly magnetic Fe–Si–Al phases rather than with strongly magnetic oxides. Consistent with Pan et al. (2020) and Abaka-Wood et al. (2022), these results indicate that magnetic separation serves best as a pre-concentration step to remove Fe-rich impurities and produce REE-enriched intermediates for subsequent chemical leaching.

3.2. Chemical Separation

The chemical separation of REEs from bottom ash was performed through a two-stage leaching sequence, consisting of an alkaline pre-treatment followed by acid leaching. The alkaline step served as a crucial pre-treatment designed to enhance REE solubility by disrupting the aluminosilicate glassy matrix in which REEs are physically and chemically trapped due to high-temperature combustion. The breakdown of this matrix increases the accessibility of REEs for subsequent acid dissolution.

Experiments were conducted on the raw material and two size fractions (-0.3 mm and -0.106 mm) to examine the influence of particle size on leaching behavior. The alkaline leaching stage

was carried out under identical conditions for all samples, using 5 mol/L NaOH at 90°C for 4 hours with a liquid-to-solid ratio of 8:1. Following this pre-treatment, acid leaching was applied at varying HCl concentrations (3, 4, and 5 mol/L) to evaluate the combined effects of acid strength and particle size on REE recovery efficiency. The final process flow diagram representing the beneficiation and leaching procedures applied to the bottom ash sample under optimized leaching conditions is presented in Figure 3.

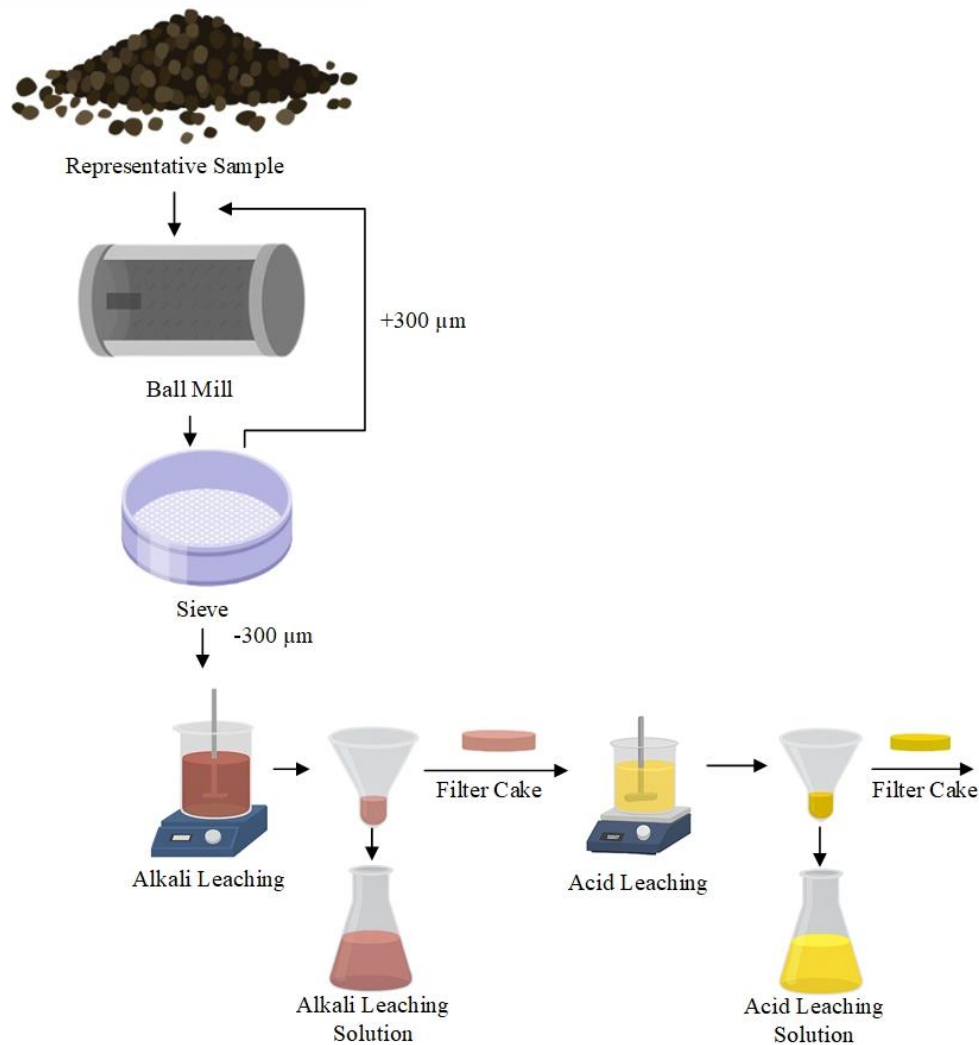


Figure 3. Process flow diagram illustrating the sequential beneficiation and leaching steps applied to the bottom ash sample under optimized leaching conditions.

3.2.1. Alkaline pre-treatment

The alkaline leaching experiments conducted on the -0.3 mm and -0.106 mm fractions revealed pronounced differences in the mass of leach residues, indicating varying degrees of matrix alteration and phase transformation. The raw feed (~ 1 mm) exhibited a moderate mass increase

from 50 g to 54.2 g (8.4%), whereas finer fractions showed substantially higher gains: the -0.3 mm fraction increased to 62.2 g (24.4%), and the -0.106 mm fraction reached 70.1 g (40.2%). This increase is primarily attributed to the in-situ formation of insoluble sodium aluminosilicates, resulting from reactions between the aluminosilicate glassy matrix and the NaOH solution. In addition, chemisorption of hydroxide ions likely contributes to the mass gain by incorporating hydroxyl species into the matrix structure. The more pronounced effect in finer fractions can be explained by their higher specific surface area and greater reactivity, which enhance alkali-induced depolymerization of the aluminosilicate network that entraps rare earth elements (REEs). The partial dissolution and structural degradation of aluminosilicate phases play a critical role in improving subsequent acid leaching efficiency by increasing the exposure and mobility of REEs. These results are consistent with findings by Li et al. (2022), who reported that alkaline attack on silicate minerals disrupts the crystal lattice and facilitates REE liberation during subsequent acid treatment.

The observed increase in residue mass therefore reflects the progressive disintegration of the coal ash matrix and formation of secondary sodium-bearing phases. The corresponding variations in the oxide composition of the feed, -0.3 mm, and -0.106 mm fractions after alkaline leaching are presented in Figure 4. A slight reduction in SiO₂, Al₂O₃, and Fe₂O₃ concentrations was observed, indicating partial dissolution of these oxides. Conversely, a substantial increase in Na₂O content was detected across all samples, attributed to residual or adsorbed NaOH and the incorporation of sodium into newly formed aluminosilicate phases. Although the apparent oxide concentrations decrease, the overall oxide mass in the residues increases when accounting for the mass gains of 8.4%, 24.4%, and 40.2% for the feed, -0.3 mm, and -0.106 mm samples, respectively. This trend confirms the formation of insoluble sodium aluminosilicates and hydroxide chemisorption as dominant mechanisms.

Figure 4 illustrates the \sum REE content in the residues, which decreases progressively with decreasing particle size, suggesting preferential dissolution or transformation of REE-bearing phases under alkaline conditions. The \sum REE content of the untreated raw sample provides a baseline for assessing subsequent acid leaching efficiency.

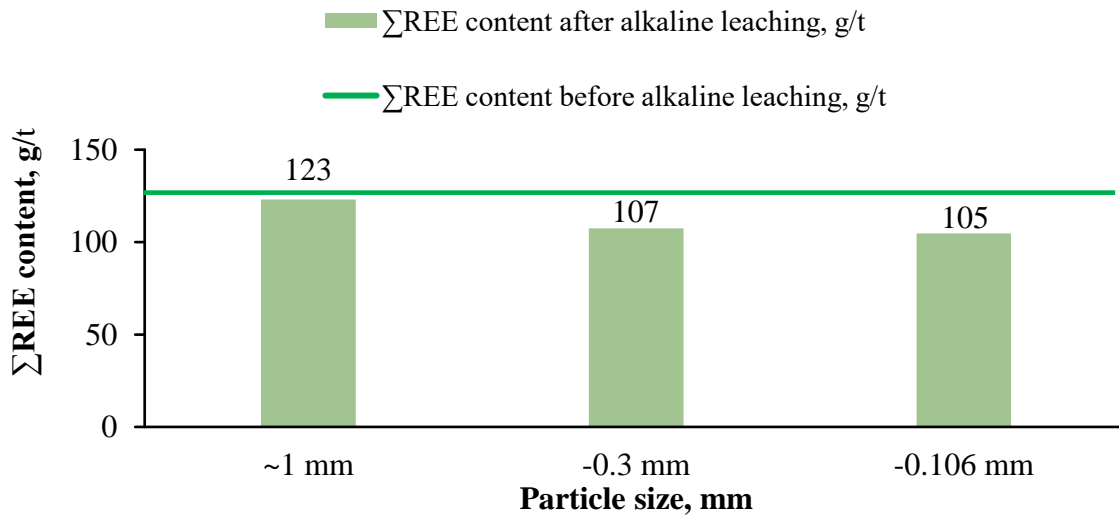


Figure 4. Effect of particle size on the variation of Σ REE content after alkaline leaching.

The progressive decline in Σ REE concentrations observed with decreasing particle size from 123 g/t in the coarse fraction to 105 g/t in the finest indicates that the alkaline leaching process did not achieve complete fixation of rare earth elements within the solid residue matrix. Instead, the enhanced reactivity and larger specific surface area of finer particles likely facilitated the structural breakdown of the amorphous aluminosilicate network, promoting partial REE mobilization into the leachate phase. This observation is consistent with the findings of Kim et al. (2024), who demonstrated that the disintegration of glassy silicate matrices under alkaline conditions accelerates REE release from structurally bound sites. Furthermore, Shoppert et al. (2020) reported that sodium hydroxide preferentially attacks the amorphous silicate phase of coal fly ash, generating reactive sodium aluminosilicate intermediates and consequently increasing REE transfer pathways toward the aqueous phase. In agreement with these mechanisms, Jyothi et al. (2020) emphasized that while secondary resources such as coal combustion residues represent promising feedstocks for REE recovery, process optimization must balance the extent of structural decomposition with the selective fixation of REEs in the solid residue to minimize leaching-induced losses.

3.2.2. Acid leaching

Acid leaching is the most widely applied technique in REE recovery, primarily relying on chemical interactions between acidic solutions and REE-bearing phases. Although various acids such as sulfuric, nitric, and organic acids have been investigated, hydrochloric acid (HCl) remains the most efficient reagent due to its strong proton activity and ability to form stable REE-chloride complexes (Zhang et al., 2015). Following the alkaline pretreatment, acid

leaching was applied to the leach residues obtained from the ~1 mm, -0.3 mm, and -0.106 mm size fractions to mobilize the residual REEs into the acid solution.

The leaching outcomes (Figure 5) unequivocally demonstrate that both acid molarity and particle size distribution control the overall efficiency and selectivity of Σ REE extraction from alkali-activated coal ash residues. The Σ REE recovery exhibited a systematic rise from 77 % at 3 M HCl to 87 % at 5 M HCl, with the finest fraction (-0.106 mm) yielding the highest recovery. This improvement is attributed to the enlarged specific surface area, reduced diffusion path length, and enhanced exposure of REE-bearing mineral phases to the reactive lixiviant (Ruan et al., 2019; Mokoena et al., 2022). Such behavior aligns with previous reports highlighting that elevated proton activity and finer particle size markedly accelerate both dissolution kinetics and the formation of chloride complexes during hydrometallurgical processing of coal-derived materials (Pan et al., 2021). The preceding alkaline pretreatment step plays a critical mechanistic role by producing highly reactive Na-Al-Si aluminosilicate domains that disrupt the polymerized silicate framework. This structural weakening facilitates proton penetration and enhances the liberation of REE species during subsequent acid leaching (Kim et al., 2024). As the acid concentration increases, cleavage of Na-O-Si and Al-O-Si bonds intensifies, improving REE solubilization while simultaneously inducing limited co-dissolution of Fe-, Ca-, and Al-bearing oxides. In contrast, the SiO₂ content of the post-leach residues displays an inverse correlation with Σ REE recovery slightly decreasing at 4 M HCl and plateauing at 5 M HCl implying that although amorphous silica domains undergo localized attack, the crystalline and polymerized silicate network remains largely chemically inert (Bagheri et al., 2022). This response exemplifies the intrinsic trade-off between REE recovery and matrix integrity, a phenomenon widely acknowledged in the hydrometallurgical extraction of REEs from coal combustion by-products (Modiga et al., 2024; Thomas et al., 2024). Consequently, the optimum operational regime is defined not by the absolute dissolution yield but by the thermodynamic and kinetic balance between extraction efficiency and phase selectivity. Under the conditions of 4 M HCl and -0.3 mm particle size, Σ REE recovery attains approximately 85 %, while more than 75 % of SiO₂ remains immobilized within the leach residue. This regime ensures efficient REE liberation with minimal matrix degradation, reduced impurity solubilization, and enhanced downstream processability underscoring the necessity of controlling both acid molarity and particle size to achieve a sustainable, selective, and industrially scalable leaching process.

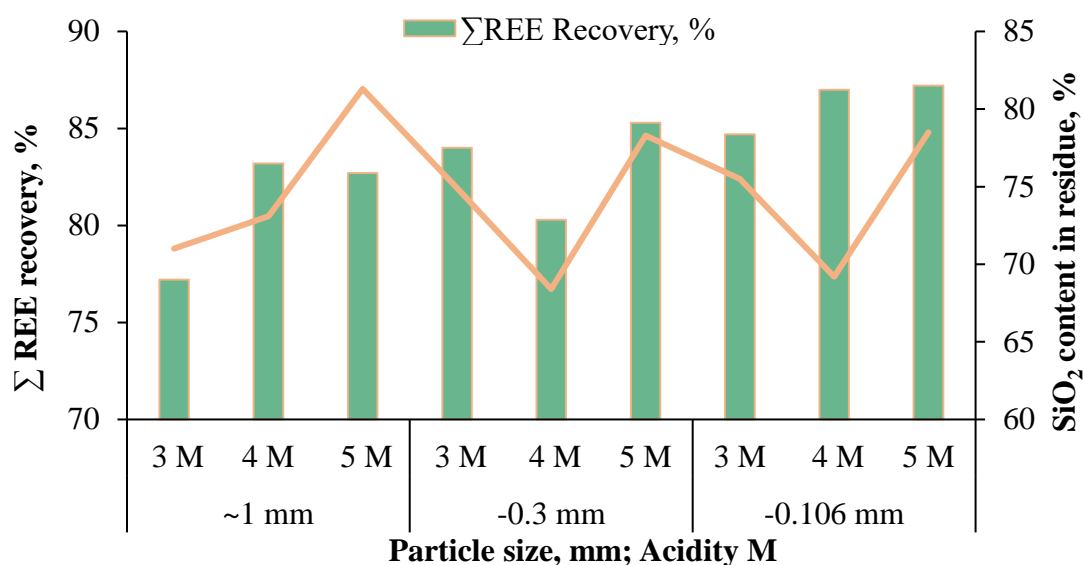


Figure 5. Combined influence of acid concentration and particle size on Σ REE recovery and SiO_2 retention during hydrochloric acid leaching of alkali-treated ash.

4. Conclusion

Coal combustion residues represent both an environmental concern and a potential resource for REE recovery. This study demonstrated that bottom ash from the Soma Thermal Power Plant contains recoverable REEs primarily bound to aluminosilicate matrices. Physical beneficiation methods (jigging, shaking table, centrifugal and magnetic separations) yielded only minor enrichment, confirming limited liberation of REE-bearing phases. Sequential alkaline and acid leaching proved significantly more effective. Alkaline pretreatment with 5 mol/L NaOH (90 °C, 4 h) partially decomposed the glassy matrix, enhancing REE accessibility, while subsequent HCl leaching achieved Σ REE recoveries exceeding 80%. Although 5 M HCl and -0.106 mm conditions yielded the highest dissolution, excessive acidity caused non-selective leaching and matrix degradation. In contrast, 4 M HCl and -0.3 mm offered an optimal compromise between recovery, selectivity, and structural stability, representing the most sustainable leaching condition.

Overall, the results confirm that physical beneficiation alone is inadequate, whereas integrated chemical processing provides a viable and scalable pathway for REE recovery from Turkish coal ashes. Given Türkiye's extensive lignite resources and ongoing thermal power generation, such residues represent abundant, low-cost, and domestically available secondary sources of critical materials. Valorization of these by-products can reduce dependence on imported REEs

and contribute to circular economy initiatives. Future studies should extend similar approaches to fly ash and coal washing residues, which also possess considerable REE potential, to establish a comprehensive strategy for sustainable critical material recovery from Türkiye's coal-based energy sector.

Acknowledgements

We thank the suppliers, TKİ, and the Soma Thermal Power Plant managers for providing the bottom ash samples used in this study.

We are also grateful to the TENMAK/NATEN project team, the ITU Department of Mineral Processing Engineering project team, and the Esan R&D Center for their valuable technical and analytical support within the scope of this project.

Author Contributions

Conceptualization, F.B.; T.U.; validation, F.B.; T.U.; N.İ.D.; G.G.; Y.E.P. A.E.Y.; investigation, F.B.; T.U.; N.İ.D.; writing—original draft preparation, F.B.; T.U.; N.İ.D.; writing—review and editing, F.B.; T.U.; N.İ.D.; G.G.; B.S.S.; visualization, F.B.; T.U.; N.İ.D.; and supervision, F.B.; T.U.; N.İ.D.; G.G.; Y.E.P. and B.S.S. All authors have read and agreed to the published version of the manuscript.

Declaration of Interest Statement

This study is coordinated and financially supported by TENMAK NATEN and TKİ [Project No: A2.H1.P22]. The authors declare that they have no additional financial or personal relationships that could have influenced the work reported in this paper.

Data Availability Statement

The data supporting the findings of this study are part of the project coordinated by TENMAK NATEN and TKİ [Project No: A2.H1.P22], conducted in collaboration with Department of Mineral Processing Engineering, Istanbul Technical University (ITU) and Esan R&D Center. Process data and analytical results can be obtained from the corresponding author upon reasonable request and with the consent of the project coordinators.

Funding

This work was supported by the TENMAK NATEN and TKİ under Project No: A2.H1.P22.

References

- Abaka-Wood, G. B., Addai-Mensah, J., & Skinner, W. (2022). The concentration of rare earth elements from coal fly ash. *Journal of the Southern African Institute of Mining and Metallurgy*, 122(1), 21-28.
- Alan, H., Ateşoğulları, M., Çağlan, D., İlgün, F., Konuk, R., & Uytun H. (2014). Manisa- Soma Eynez Karanlıkdere Mevkii Kapalı Ocak Kömür Madeni İşletmesi İş Cinayeti/İş Kazası Raporu. TMMOB Jeoloji Mühendisleri Odası Yayınları.
- Bagheri, M., Lothenbach, B., Shakoorioskooie, M., & Scrivener, K. (2022). *Effect of different ions on dissolution rates of silica and feldspars at high pH*. *Cement and Concrete Research*, 152, 106644. <https://doi.org/10.1016/j.cemconres.2021.106644>
- Dai, S., Ren, D., Chou, C. L., Finkelman, R. B., Seredin, V. V., & Zhou, Y. (2012). Geochemistry of trace elements in Chinese coals: A review of abundances, genetic types, impacts on human health, and industrial utilization. *International Journal of Coal Geology*, 94, 3-21. <https://doi.org/10.1016/j.coal.2011.02.003>
- Gao, L., and Y. Chen. (2010). A study on the rare earth ore containing scandium by high gradient magnetic separation. *Journal of Rare Earths* 25: 623–626.
- Honaker, R., Groppo, J., Bhagavatula, A., Rezaee, M., & Zhang, W. (2016). Recovery of rare earth minerals and elements from coal and coal byproducts. In *International Conference of Coal Preparation*, Louisville, Kentucky (pp. 25-27).
- Jyothi, R. K., Thenepalli, T., Ahn, J.-W., & Lee, J.-Y. (2020). *Review of rare earth elements recovery from secondary resources for clean energy technologies: Grand opportunities to create wealth from waste*. *Journal of Cleaner Production*, 267, 122048. <https://doi.org/10.1016/j.jclepro.2020.122048>
- Karayigit, A. I., Gayer, R. A., Querol, X., & Onacak, T. (2000). Contents of major and trace elements in feed coals from Turkish coal-fired power plants. *International Journal of Coal Geology*, 44(2), 169-184.
- Kim, G. M., Park, S., Choi, J., Park, S., & Kim, J. (2024). *Effects of alkaline extraction on the behavior of rare earth elements in coal ashes*. *Environmental Science and Pollution Research*, 31, 63210–63224. <https://doi.org/10.1007/s11356-024-34943-x>
- King, J.F., Taggart, R.K., Smith, R.C., Hower, J.C., & Hsu-Kim, H. (2018). Aqueous acid and alkaline extraction of rare earth elements from coal combustion ash. *International Journal of Coal Geology*. <https://doi.org/10.1016/j.coal.2018.05.009>.

- Lin, R., Howard, B. H., Roth, E. A., Bank, T. L., Granite, E. J., & Soong, Y. (2017). Enrichment of rare earth elements from coal and coal by-products by physical separations. *Fuel*, 200, 506-520.
- Modiga, A., Eterigho-Ikelegbe, O., & Bada, S. (2024). *Extractability and mineralogical evaluation of rare earth elements from high-ash discard coal*. *International Journal of Coal Science & Technology*, 11, 65. <https://doi.org/10.1007/s40789-024-00702-z>
- Mokoena, K., Mokhahlane, L. S., & Clarke, S. (2022). *Effects of acid concentration on the recovery of rare earth elements from coal fly ash*. *International Journal of Coal Geology*, 259, 104037. <https://doi.org/10.1016/j.coal.2022.104037>
- MTA, (2017). *Dünyada ve Türkiye’de nadir toprak elementleri (nte)*. Maden Serisi: 5, Fizibilite Etütleri Daire Başkanlığı, Ankara.
- Pan, J., Hassas, B. V., Rezaee, M., Zhou, C., & Pisupati, S. V. (2021). *Recovery of rare earth elements from coal fly ash through sequential chemical roasting, water leaching, and acid leaching processes*. *Journal of Cleaner Production*, 284, 124725. <https://doi.org/10.1016/j.jclepro.2020.124725>
- Pan, J., Nie, T., Hassas, B. V., Rezaee, M., Wen, Z., & Zhou, C. (2020). Recovery of rare earth elements from coal fly ash by integrated physical separation and acid leaching. *Chemosphere*, 248, 126112.
- Ruan, Z., Li, M., Gao, K., Zhang, D., Huang, L., Xu, W., & Liu, X. (2019). *Effect of particle size refinement on the leaching behavior of mixed rare-earth concentrate using hydrochloric acid*. *ACS Omega*, 4(4), 8395–8402. <https://doi.org/10.1021/acsomega.9b01141>
- Shoppert, A., Valeev, D., Loginova, I., & Chaikin, L. (2020). *Complete extraction of amorphous aluminosilicate from coal fly ash by alkali leaching under atmospheric pressure*. *Metals*, 10(12), 1684. <https://doi.org/10.3390/met10121684>
- Stoy, L., Diaz, V., & Huang, C. H. (2021). Preferential recovery of rare-earth elements from coal fly ash using a recyclable ionic liquid. *Environmental Science & Technology*, 55(13), 9209-9220.
- Thomas, B. S., Dimitriadis, P., Kundu, C., Vuppaladadiyam, S. S. V., Raman, R. S., & Bhattacharya, S. (2024). *Extraction and separation of rare earth elements from coal and coal fly ash: A review on fundamental understanding and on-going*

engineering advancements. Journal of Environmental Chemical Engineering, 12(3), 112769. <https://doi.org/10.1016/j.jece.2024.112769>

Trinh, H. B., Kim, S., & Lee, J. (2022) Recovery of rare earth elements from coal fly ash using enrichment by sodium hydroxide leaching and dissolution by hydrochloric acid, *Geosystem Engineering*, 25:1-2, 53-62. DOI: 10.1080/12269328.2022.2120092 .

Url-1 < <https://somatermik.com.tr/Tr/kurumsal> >. erişim tarihi 12.09.2025.

Url-2 < <https://www.astm.org/d6357-21b.html> >, erişim tarihi 10.09.2025.

Wang, Z., Dai, S., Zou, J., French, D., & Graham, I. T. (2019). Rare earth elements and yttrium in coal ash from the Luzhou power plant in Sichuan, Southwest China: Concentration, characterization and optimized extraction. *International Journal of Coal Geology*, 203, 1-14.

Wen, Z., Zhou, C., Pan, J., Cao, S., Hu, T., Ji, W., & Nie, T. (2020). Recovery of rare-earth elements from coal fly ash via enhanced leaching. *International Journal of Coal Preparation and Utilization*, 2041-2055. doi:10.1080/19392699.2020.1790537.

Whateley, M. K. (1995). Soma Lignite Basin, Turkey. *Introduction to Mineral Exploration*, 294.

Zhang, W., Honaker, R. Q., & Groppo, J. (2020). A review of the recovery of rare earth elements from coal combustion by-products. *Minerals*, 10(5), 451.

Zhang, W., Honaker, R., & Groppo, J. (2017). Concentration of rare earth minerals from coal by froth flotation. *Minerals & Metallurgical Processing*, 34, 132-137.

Zhang, W., Rezaee, M., Bhagavatula, A., Li, Y., Groppo, J., & Honaker, R. (2015). A review of the occurrence and promising recovery methods of rare earth elements from coal and coal by-products. *International Journal of Coal Preparation and Utilization*, 35(6), 295-330.

TABLES

Table 1. The main oxide compositions and contents of the BA.

Major elements (wt.%)			
CaO	38,6	MgO	2,1
SiO ₂	29,9	K ₂ O	0,8
Al ₂ O ₃	9,4	TiO ₂	0,3
Fe ₂ O ₃	8,2	Na ₂ O	0,5

Table 2. REE contents of the BA.

Elements	Sc**	La**	Ce**	Pr**	Nd**	Sm**	Ey*	Gd*	
Content (g/t)	0.23	24.97	37.23	4.68	18.98	3.74	1.06	3.26	
Elements	Tb*	Dy*	Ho*	Er*	Tm*	Yb*	Lu*	Y*	∑REE***
Content (g/t)	0.51	2.80	0.57	1.68	0.27	0.27	1.62	16.26	122.7

*HREE: Heavy Rare Earth Elements; **LREE: Light Rare Earth Elements; ***∑REE: Total REE

Table 3. Alkaline leaching and acid leaching test conditions.

Leaching test conditions				
Alkaline Leaching (NaOH)	Concentration, mol/L	5 mol/L		
	Temperature, °C	90°C		
	Time, h	4 h		
	Liquid: Solid ratio	8:1		
Acid Leaching (HCl)	Concentration, mol/L	3 mol/L	4 mol/L	5 mol/L
	Temperature, °C	90°C	90°C	90°C
	Time, h	3 h	3 h	3 h
	Liquid: Solid ratio	10:1	10:1	10:1

Table 4. Jig test result at + 1 mm size.

Products	Amount, %	Ash, %	∑LREE, g/t	∑HREE, g/t	∑REE, g/t	∑REE Distribution, %
Heavy 1	22.6	95.7	17	39	56	14.8
Heavy 2	21.0	93.8	20	51	71	17.4
Middling	38.1	92.3	23	61	84	37.4
Light 1	8.1	75.7	34	94	128	12.1
Light 2	10.2	81.9	40	114	154	18.3
Total	100.0	91.0	24	62	86	100.0

Table 5. Soma Thermal Power Plant bottom ash sample magnetic separation test results.

Particle size, mm	Amount, %	Products	Content REE, g/t	Distribution, %	Ash, %	According to the experiment	
						REE content, g/t	REE Distribution, %
-1+0.5 (REMS)	28.7	Magnetic	190	1.9	95.9	182	2.4
		Middling	179	16.3	95.4	171	20.9
		Non-Magnetic	61	4.3	94.3	58	5.5
		Total	131	22.5	95.0	124	28.8
-0.5+0.212 (REMS)	37.0	Magnetic	206	5.0	93.7	193	5.1
		Middling	203	24.0	91.7	186	24.2
		Non-Magnetic	97	7.7	91.0	88	7.7
		Total	166	36.7	91.6	152	37.0
-0.212 (Carpco)	34.3	Magnetic	313	9.4	95.2	298	8.2
		Middling	351	3.4	92.9	326	2.6
		Non-Magnetic	169	28.0	91.1	154	23.4
		Total	199	40.8	91.8	182	34.2
Total	100.0		167	100.0		154	100

FIGURES

Figure 1. XRD analysis of BA.

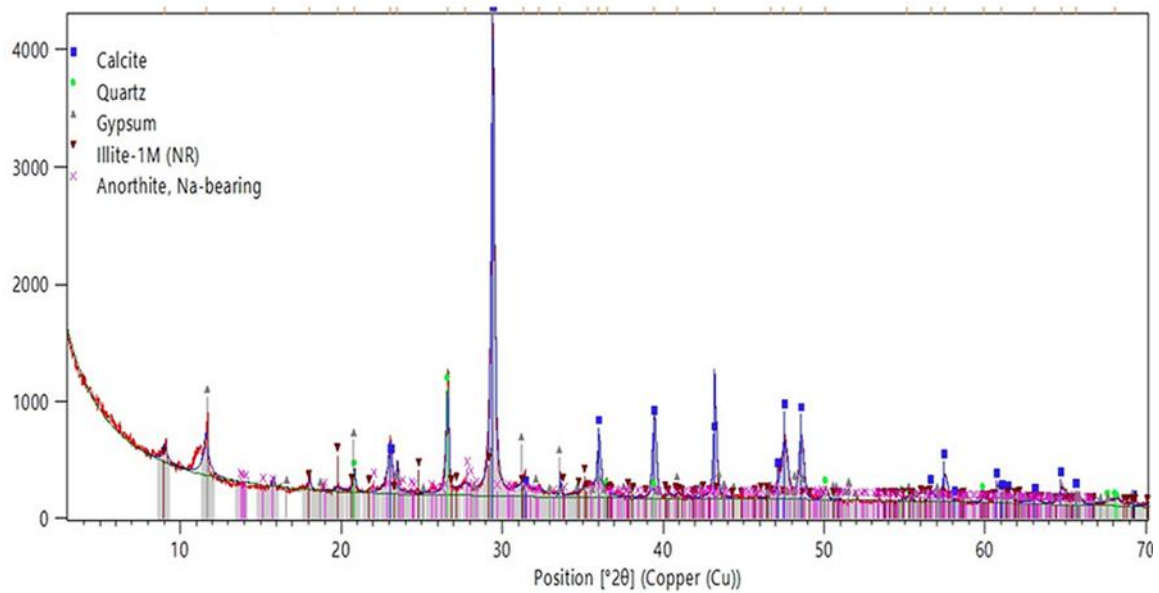


Figure 2. Combined major oxide and Σ REE contents across particle size fractions of the BA.

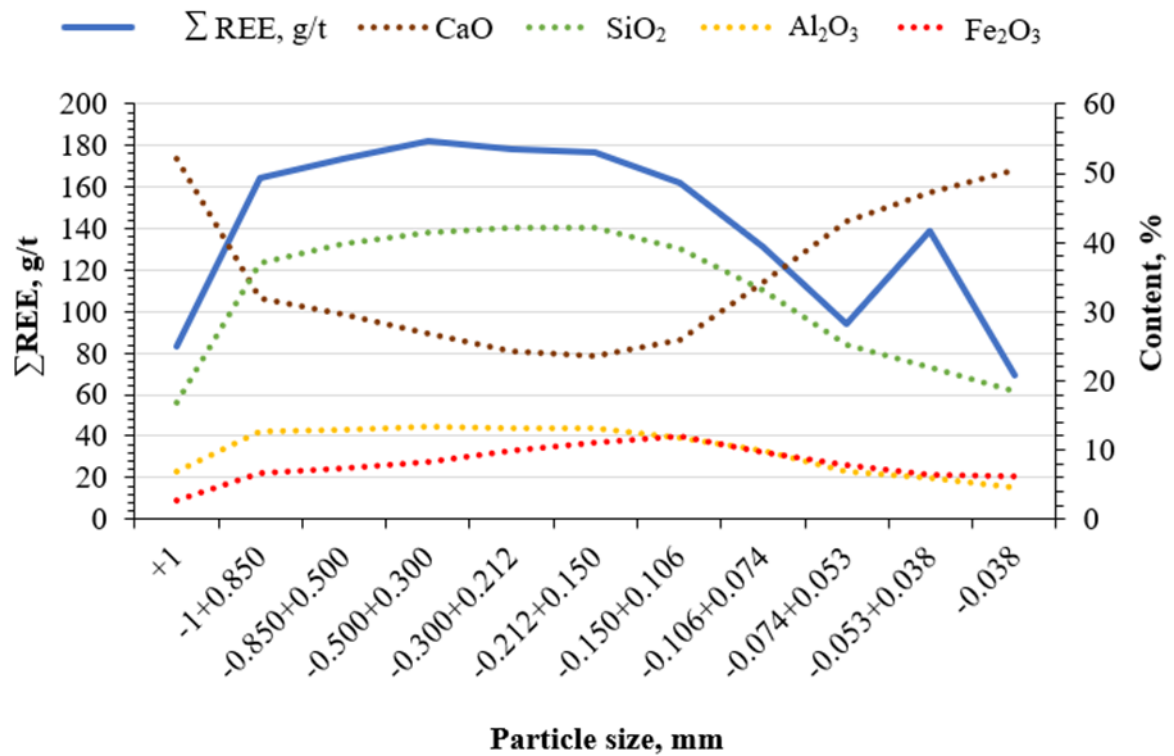


Figure 3. Process flow diagram illustrating the sequential beneficiation and leaching steps applied to the bottom ash sample under optimized leaching conditions.

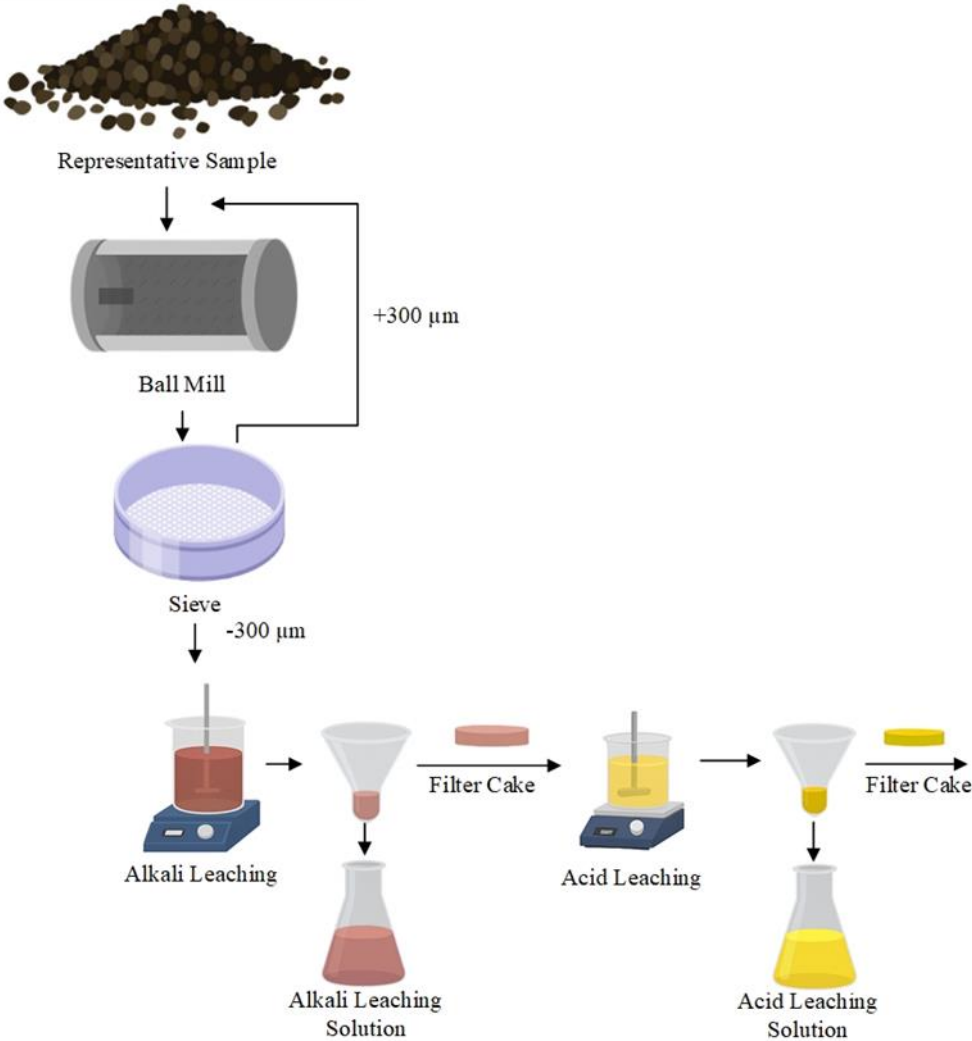


Figure 4. Effect of particle size on the variation of Σ REE content after alkaline leaching.

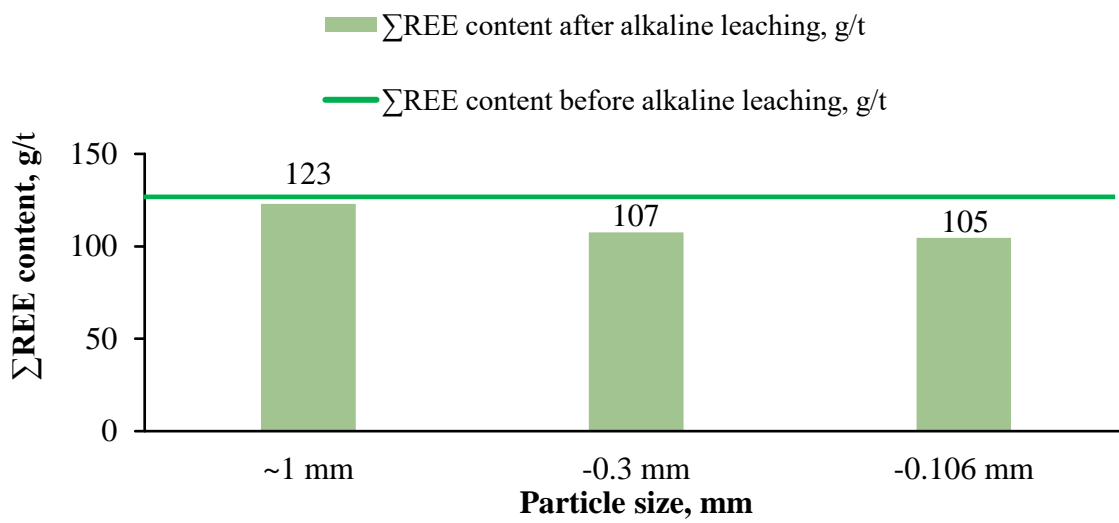


Figure 5. Combined influence of acid concentration and particle size on Σ REE recovery and SiO_2 retention during hydrochloric acid leaching of alkali-treated ash.

